Title : **Feasibility of motion estimation and tracking in portal images during treatment of pulmonary cancers by conformal radiotherapy**

Authors : Maciej Orkisz [1], Anne Frery [1], Bruno Durning [1], Olivier Chapet [2], Françoise Mornex [2], Isabelle E. Magnin [1]

Affiliations : [1] *CREATIS, CNRS Research Unit #5515 affiliated to INSERM, Lyon, France*
[2] *Dept. of Radiotherapy Oncology, Lyon-South Hospital, Pierre Bénite, France*

Address : CREATIS, INSA de Lyon
Bât. Blaise Pascal
7 rue J. Capelle
F-69621 Villeurbanne cedex
France

Acknowledgements : This work is in the scope of the scientific topics of the GDR-PRC ISIS research group of the French National Center for Scientific Research (CNRS). The authors are grateful to Arnaud Ruillère for his help in acquisition of images of phantoms.

Abstract : Medical objective of this work is to compensate tumor's displacements due to free breathing, so as to reduce the irradiated zone and thus preserve healthy tissues. For this purpose, we are studying the feasibility of tracking the tumor's motion in portal images, *i.e.* in images generated by the treatment beam (high-energy X-rays). Two reference algorithms were tested on sequences of portal images of a phantom and of patients. Target tracking algorithm (block-matching), was able to correctly track the target only when the tumor was perceptible in the images. Otherwise it would require implanting of radio-opaque markers in tumor's vicinity. Optical flow estimation was expected to deduce "invisible" tumor's displacements from the motion of neighboring tissues. However, the standard Horn & Schunck's algorithm gave poor results because of low contrast and absence of texture in the images. We are suggesting a modified version of this approach, based on intersections of motion constraint lines for a limited number of pixels carrying reliable and complementary motion information.

Keywords : conformal radiotherapy, medical imaging, image sequence, motion estimation, target tracking, cancer

1. Introduction

To sterilize bronchial cancers effectively, a high dose of radiation is to be delivered in the volume containing pathological tissues, while avoiding irradiation of the healthy neighboring tissues. The volume to be irradiated is determined by an expert from scanner images and contains a margin [ARM'98], so as to cope with: 1) the uncertainties on the exact limits of the tumor and 2) the errors of repositioning of the patient from one radiotherapy session to another. Conformal radiotherapy provides two mechanisms to protect neighboring healthy tissues as well as possible, while destroying cancerous cells [MOR'99]. On the one hand, the treatment beam orientation varies during the radiotherapy session, while focusing in the tumor region (fig.1). On the other hand, the collimator of the accelerator is provided with mobile leaves which mask the healthy tissues (fig.2a). A custom mask can also be used (fig.2b). To make coincide the planned irradiation zone with the actual tumor, the patient is repositioned at the beginning of each radiotherapy session by means of an immobilizing matrix and of external marks. Accuracy of the repositioning can be verified using an electronic portal imaging device (EPID) [MOR'96]. The portal images are generated by the treatment beam itself, on a sensor placed behind the patient's body. However, few sensors accept the very high energy level of the ionizing beam (typically between 6 and 15 MeV) and provide a sufficiently contrasted image. Only some natural landmarks, such as bones, are approximately perceptible. This is not sufficient for soft organs such as prostate, which can move slightly from one day to another compared to the bones. In this case, an artificial marker can sometimes be implanted, in the tumor or in its vicinity, so as to facilitate its locating.

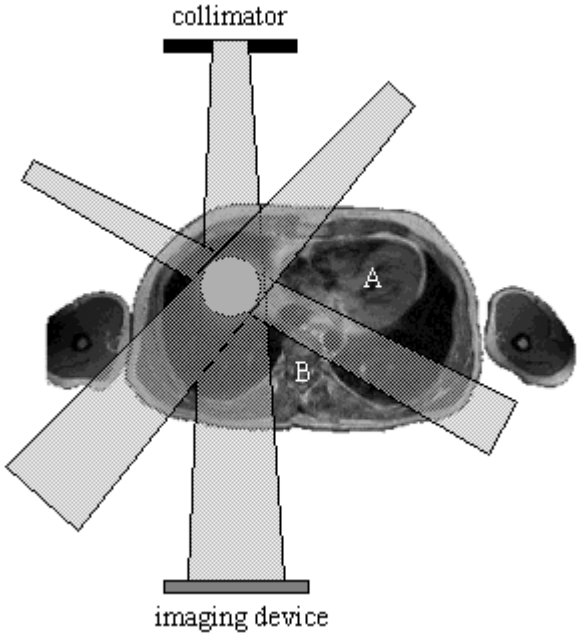

Figure 1 : Scanner cross-section of human thorax with a schematic representation of a radiotherapy treatment setup. An electronic portal imaging device (EPID) can be placed in front of the collimator and moved around the patient, following the beam orientation changes. Planned beam orientations avoid irradiation of vital organs such as heart (A) and spine (B).

a) 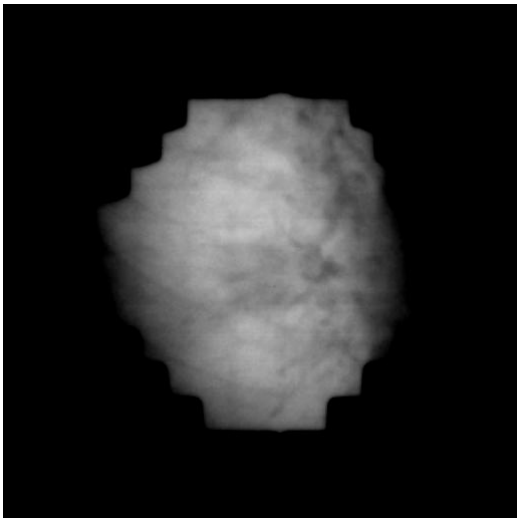 b) 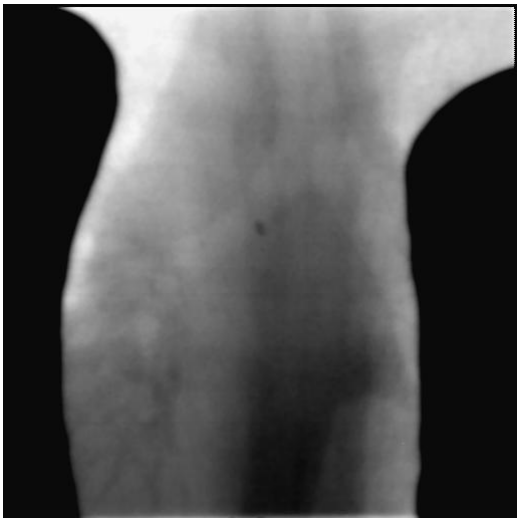

Figure 2 : Bronchial zone portal images obtained by IRIS (Bio-Scan s.a., Geneva, Switzerland). Black forms correspond to the regions protected by: collimator leaves (a), custom mask (b). In the image (a) tumor is exceptionally perceptible as a darker spot in the center. In the image (b) tumor is not perceptible, but neighboring organs can be recognized, especially bronchi (brighter inverted Y-shape). Dark small spot in the center is a metal marker stuck on the patient's skin.

The above described technique suits the treatment of the tumors located on organs which do not move during the radiotherapy session. For moving organs such as lungs, one solution is an enlargement of the irradiation zone, so as to cover all the amplitude of displacement. The extreme locations of the tumor can be determined using scanner images respectively acquired at end-expiration and end-inspiration [MAH'99]. However, the benefits acquired by the conformal radiotherapy are then reduced, since some healthy tissues inevitably enter the maximally irradiated zone. Another solution is to switch on and off the irradiating beam synchronously with breathing [KUB'99] [MAH'99]. The patients are usually "trained" to carry out regular breath-holds. A spirometer or another monitoring device is used to detect the patient's state (apnea or breathing) and to automatically start and stop the irradiation in consequence. However, reproducible deep inspiration breath-holds are difficult for the patients with pulmonary lesions, whose respiratory capacities are decreased, and only a minority of them is able to correctly perform the necessary maneuver.

The objective of our study is to develop a system capable of tracking the tumor motion in real time, so as to automatically control the position of the beam or of the patient. We took as a starting point the existing techniques of image processing and, in particular, a software developed within our laboratory, called Echotrack [ORK'98] [ORK'99]. This software succeeds in tracking in real time the motion (induced by breathing and by patient's movements) of renal stones perceptible in ultrasound images, and automatically adjusts the position of the generator of shock waves according to the displacements of the stone. However, ultrasound is not suitable for pulmonary imaging, due to air contained in lungs.

Instead, the use of portal images seems to be a good solution, since it avoids additional equipment and additional dose of ionizing radiation that would occur when using fluoroscopy, for example [SHI'99]. Although conventional EPIDs provide very low-contrast images and their imaging rate is not sufficient, compared with the breathing rate, our project is based on a new-generation system called IRIS (Interactive Radiotherapy Imaging System, Bio-Scan s.a., Geneva, Switzerland). This imaging device performs frame grabbing of better quality and at a much higher acquisition rate (up to 12 images a second) than the conventional EPIDs.

Our project is at the stage of a feasibility study. Let us note that portal images (fig. 2) have photometrical characteristics (contrasts, dynamics, noise…) which strongly differ from the video images. Given that motion estimation and tracking algorithms reported in literature generally were developed in the context of video image sequences, the first step was to test the applicability of "gold standard" algorithms from the video field, to the portal image sequences. The second step was to propose application-tailored improvements. In the sequel of this paper, firstly two approaches based on block matching and on motion constraint equation (differential appproach) will be justified, then the tests carried out will be described, lastly the results and perspectives will be discussed.

2. Methods

We are exploring two directions. The first one is based on the assumption according to which the tumour can be highlighted in the images, *e.g.* by implanting gold markers, like in the case of the prostate. Although currently this process is not clinically available for the lungs, such an attempt was recently reported [SHI'99]. The use of target tracking algorithms based on block-matching should then be possible. The second direction is based on a realistic assumption according to which the tumor is not visible in the portal images because of an insufficient contrast between soft tissues. Provided that the motion of the surrounding organs can be determined, it should be possible to determine, by interpolation, the displacement of the tumor. This assumption leads to explore algorithms based on local spatio-temporal variations of image intensity, *i.e.* on a differential approach.

2.1. Target tracking

Usually, the target is an icon, *i.e.* a small fragment of an image. An icon is first selected (automatically or interactively) in an initial image of the considered sequence. Then a similarity criterion is used to find, in each image of the sequence, the fragment which matches the target [AGG'81]. High-level criteria of similarity, such as the criteria based on lengths and orientations of line segments, usually are more reliable than low-level ones, provided that structural information characterizing the icon can be extracted from the image data. In our case no structural information is available. Hence we are forced to choose low-level methods. These methods are generally referenced as "block matching", where a block is simply the brightness pattern of the icon. Their implementations differ from each other by the search strategy. There are also different possible choices of the similarity measure. We implemented the correlation centered on the mean value and normalized by the variance.

$$C(x,y)=\frac{\sum_{i=1}^{M}\sum_{j=1}^{N}\left[R(i,j)-\mu_r\right]\times\left[P(i,j)-\mu_p\right]}{\sqrt{\sum_{i=1}^{M}\sum_{j=1}^{N}\left[R(i,j)-\mu_r\right]^2}\times\sqrt{\sum_{i=1}^{M}\sum_{j=1}^{N}\left[P(i,j)-\mu_p\right]^2}}. \quad (1)$$

In this formula (x,y) represent the location of the currently tested block, $P(i,j)$ is the brightness of the pixel (i,j) in this block, $R(i,j)$ is the brightness of the corresponding pixel in the reference block, μ_p, μ_r are the mean values of these blocks and M, N represent the block size. This measure was also implemented in our Echotrack software, in a computationally faster version derived from (1):

$$C(x,y)=\frac{\sum_{i=1}^{M}\sum_{j=1}^{N}R(i,j)P(i,j)-MN\mu_r\mu_p}{\sqrt{\sum_{i=1}^{M}\sum_{j=1}^{N}R^2(i,j)-MN\mu_r^2}\times\sqrt{\sum_{i=1}^{M}\sum_{j=1}^{N}P^2(i,j)-MN\mu_p^2}}. \quad (2)$$

Instead of searching for a maximum of similarity, one can seek a minimum of disparity. We implemented two well-known disparity measures: sum of absolute differences and sum of squared differences (k = 1 or 2):

$$D(x,y)=\sum_{i=1}^{M}\sum_{j=1}^{N}\left|R(i,j)-P(i,j)\right|^k. \quad (3)$$

As for the search strategy, we obviously implemented an exhaustive search, which consists in scanning all the possible locations within a search window, and thus guarantees that the global optimum is found. We also tested a multi-grid strategy with progressive mesh-size reduction, called log-D step [JAI'81], used in the Echotrack. This method is much faster, but potentially sub-optimal. The search is carried out in a small number L of iterations. At each iteration l+1, the similarity criterion is calculated for eight locations around the best match location (x_l, y_l) from the iteration l: $(x_l + \Delta_{l+1}, y_l + \Delta_{l+1})$, $\Delta_{l+1} \in \{-d_{l+1}, 0, d_{l+1}\}$. Distance between these locations (mesh-size) is first equal to $d_1 = 2^{L-1}$, then $d_{l+1} = d_l/2$, $l+1 \in \{2,..,L\}$. At the first iteration, the similarity criterion is also calculated for the location (x_0, y_0) corresponding to the target position in the previous image or to its predicted position, in the case of predictable movements. Three iterations are sufficient to estimate the displacements for normal breathing and usual imaging conditions. Indeed, the in-plane movement of lungs can be approximately considered as sinusoidal with a typical frequency of 12 breaths per minute. The maximum peak-to-peak displacement (observed for the lower part of the lungs) reaches 40 mms. For an acquisition rate of 5 images per second (which is not the maximum rate available with IRIS, but higher rates may decrease image quality), it can be calculated that the maximum displacement between two consecutive images is equal to 5 mms. Given the typical size of the field of view and the resolution of the image acquisition matrix, we have 1 mm = 1 pixel. Hence, we need to estimate displacements up to 5 pixels. With L = 3 the maximum displacement which can be estimated, is equal to 7 pixels ($d_1 + d_2 + d_3 = 4 + 2 + 1$). The number of scanned locations is then only 25, while 225 locations would be scanned for the exhaustive search within a window of equivalent size.

2.2. Optical flow estimation

Within the differential approach, the reference method is the one proposed by Horn and Schunck [HOR'81]. Generally, each new algorithm is compared to the Horn and Schunck's one, so as to show the improvements achieved [BAR'94]. Most of these improvements attempt to cope with motion field discontinuities which are frequent in video images [ORK'96]. However, in a first approximation, motion of different organs and tissues within the human body can be considered as continuous. Indeed, "static" organs (liver, kidneys …) undergo movements induced by the neighboring "moving" organs (heart, lungs) and the amplitude of this motion decreases "continuously", as the distance from the heart or lungs increases and the distance to the bones decreases. Moreover, given the low contrasts in the portal images of the thorax, motion discontinuities (if any) would not appear as clean breaks. That is why we chose to test the Horn and Schunck's method, before seeking its improvements.

Let us remind the foundations of this method. It is based on three constraints: 1) brightness invariance of the moving points, 2) smoothness of the motion field and 3) small displacements. The first-order Taylor series development of the brightness invariance equation gives rise to the so-called motion constraint equation:

$$I_x u + I_y v + I_t = 0\,, \tag{4}$$

where I_x, I_y and I_t are the components of the spatio-temporal gradient of the brightness. This single equation is not sufficient to find two unknowns, u and v, which are the components of the velocity vector. That is why a second constraint is necessary. In the Horn and Schunck's method, the smoothness constraint is expressed using the spatial derivatives of u and v:

$$\varepsilon_c^2 = u_x^2 + u_y^2 + v_x^2 + v_y^2\,. \tag{5}$$

The motion estimation becomes an energy minimization problem with two energy terms weighted by a coefficient α, a smoothing (regularizing) term ε_c^2 and a data attachment term :

$$\varepsilon_d^2 = (I_x u + I_y v + I_t)^2\,. \tag{6}$$

The motion field is estimated by iterative minimization of the following energy functional on the image support S:

$$E = \sum_{s \in S} \varepsilon_d^2(s) + \alpha\, \varepsilon_c^2(s)\,. \tag{7}$$

This algorithm was applied to images from patients with bronchial cancer. True displacements were unknown. Hence two strategies were used to assess the consistence of the results. Firstly, motion fields obtained for each pair of consecutive images were visually inspected and compared with the perceptible movements. Secondly, the algorithm was tested on sequences with synthetic motion generated by taking one image from the original sequence and by applying to it known translations. It gave poor results for both real and synthetic motion. Significant velocity vectors were concentrated in a few regions having enough contrast to carry the motion information (fig.3). For the majority of the pixels, one can note that the spatio-temporal gradients are close to zero, which explains the null amplitudes of the

velocity vectors. The smoothness constraint makes that the iterative optimization process carries out a kind of averaging: although it propagates the motion information towards the homogeneous zones, it also reduces the amplitude of estimated displacements where the motion information is present. Moreover, the assumption of brightness invariance does not necessarily hold in portal images. In some sequences, we observed significant variations of the mean intensity, probably due to beam power fluctuations. Although these fluctuations do not significantly modify the spatial gradients of the intensity, they strongly affect the temporal derivative I_t. For all these reasons the conventional approach of Horn and Schunck seems to be unsuited. Seeing these results however, one can consider a similar method where the points taken into account for calculations would be selected according to their spatio-temporal gradients.

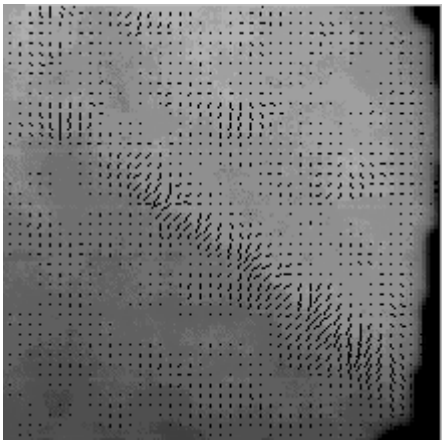

Figure 3 : Fragment of the motion field obtained by the Horn and Schunck's algorithm for a pair of images from a patient. The only region with enough contrast to carry the motion information is the boundary of the heart (near the diagonal line of this sub-image).

2.3. Intersection of motion constraint lines

It can be noted that in the system of coordinates (u, v) the motion constraint equation (4) describes a straight line called motion constraint line [SCH'89]. Actual velocity lies somewhere on this line and can be found by intersection of constraint lines corresponding to different points undergoing the same motion. Let us re-write the equation (4) for two points, in the following matrix form:

$$\begin{bmatrix} I_x^1 & I_y^1 \\ I_x^2 & I_y^2 \end{bmatrix} \begin{bmatrix} u \\ v \end{bmatrix} = - \begin{bmatrix} I_t^1 \\ I_y^2 \end{bmatrix}, \tag{8}$$

$$\mathbf{A}\mathbf{v} = -\mathbf{B}. \tag{9}$$

The intersection of constraint lines is then calculated as follows:

$$\mathbf{v} = -\mathbf{A}^{-1}\mathbf{B}. \tag{10}$$

In the case of breathing, all the points of the image are supposed to roughly undergo the same movement close to translation. However, because of noise, even for a perfect translation different pairs of constraint lines give a more or less dispersed cluster of intersections $(u_i, v_i)^T$ instead of one intersection. Moreover, spurious intersections occur when

the equation system is poorly conditioned, *i.e.* det(**A**) ≈ 0. This happens in two cases: 1) for points having similar orientations of the spatial intensity gradient, since the constraint lines are then almost parallel, 2) for points having very low values of spatial intensity gradients. For these reasons, it is necessary to calculate a kind of "mean intersection" [CHU'89], while rejecting outliers. In our experimentation we simply selected a small number (typically 30) of sufficiently spaced points (neighboring points usually have too similar gradient orientations) with sufficiently large spatio-temporal gradients. Then the intersections of the corresponding constraint lines were calculated. The global velocity vector was assigned the median value of each component of the velocity vectors deduced from each intersection, *i.e.* the estimated final velocity was equal to:

$$\hat{\mathbf{v}} = (\text{median}(u_i), \text{median}(v_i))^T. \quad (11)$$

However, more sophisticated selection criteria can be implemented, based on the value of det(**A**) [TIS'95] or on both gradient moduli and orientations. Let us note that preliminary low-pass filtering of the images was performed to reduce the influence of noise. It was also necessary to cope with the fluctuations of the mean intensity. For this purpose, a rectangle not covered by the mask was selected, its mean intensity was calculated in each image, and the intensity of each point was normalized by this mean value. The complete algorithm can be summarized as follows:

1. Selection of a non-masked region of interest (ROI).
2. For each image of the sequence, within the ROI:
   a. low-pass filtering,
   b. calculation of the mean intensity,
   c. for pixels placed on a sparse grid (step δ):
      - normalization of the intensities,
      - calculation of the spatio-temporal gradients,
      - selection of pixels with gradients greater than a threshold value τ,
      - computation of the constraint-line intersections (10),
   d. calculation of the median velocity (11).

There are two parameters: δ and τ. The grid size δ, together with the size of the ROI, determines the number of candidate points. The threshold τ defines the level of confidence in the motion information carried by these points.

3. Tests

In the sequel, the target tracking algorithm based on block matching and the differential algorithm based on intersections of motion constraint lines will be respectively referred to as BM and IMCL algorithms. The BM algorithm was first tested on images of a phantom (fig.4). This was the best means of acquiring images under conditions close to reality (contrast, noise, resolution), where the location of he target was perfectly known. We used a phantom having the same average density as the human body, and density variations simulating the internal organs (namely lungs). A metal implant approximately 3 mms in

diameter was placed inside. Breathing was simulated by table displacements controlled by electric drives. We simulated a sinusoidal movement along the head-feet line, with 40 mms of amplitude (maximum amplitude observed for the lower part of the lungs) and a frequency of 12 breaths per minute. A series of 25 static images was acquired using a conventional EPID (Varian, Palo Alto, USA), in table locations corresponding to the acquisition rate of 5 images per second, *i.e*. extent of the resulting image sequence was one breathing cycle. Then the user manually selected, in the first image, rectangles of various sizes, framing the marker. These rectangles, each one in his turn, were considered as a target and tracked using the implemented versions of the BM algorithm.

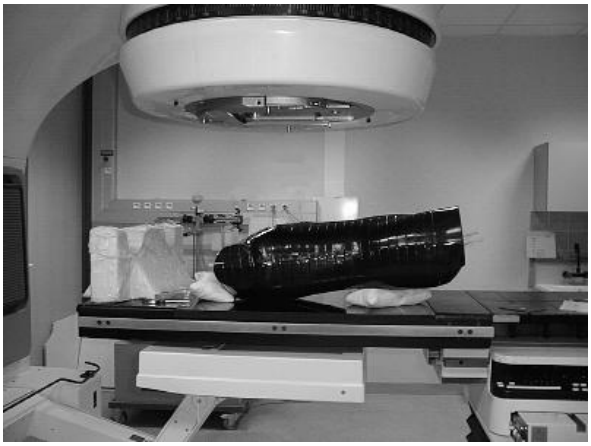

Figure 4 : Experimental setup for image acquisition of a human-body phantom. Top down : collimator of the accelerator, phantom, mobile table with position controlled by electrical drives. The imaging device is placed below the table.

The subsequent series of tests involved images of patients, acquired with IRIS (Bio-Scan s.a., Geneva, Switzerland). Since implanting markers in the bronchial region is not yet clinically available, a metal grain was stuck on the patient's skin (fig.2b). The grain was immobilized between the patient's back and the table, while the internal organs in the "background" moved normally. Hence, the tracking algorithm was supposed to find zero displacements when the selected target was containing the marker.

In one image sequence, tumor was exceptionally perceptible (fig.2a). No markers were used in this case. The displacements were unknown. The algorithm's precision was visually assessed after motion compensation, *i.e*. each image was moved according to the opposite of the estimated displacement vector and an image sequence was constructed, in which the tumor was expected to be still, provided that the displacements were correctly estimated.

As for the IMCL method, it was first checked on real images with synthetic motion, in the same manner as the Horn and Schunck's algorithm (see §2.2). Then it was tested on the sequence of 50 images with perceptible tumor (fig.2a). Since real velocities were unknown, we took as reference the displacements estimated by the BM algorithm. Although velocity and displacement are not the same thing, they can be compared since velocities are calculated with time unit equal to time interval between two consecutive images.

4. Results and discussion

Unlike the Horn and Schunck's algorithm, the BM algorithm gave satisfactory results, although the target was sometimes hardly perceptible, especially in the conventional EPID images (fig.5). The most important result is the fact that each algorithm followed the target all along its displacements, although in a few images the estimated position was not perfectly centered on the theoretical position of the marker. In images with unknown motion, tumor appeared to be immobile after compensation of the estimated displacements.

a) 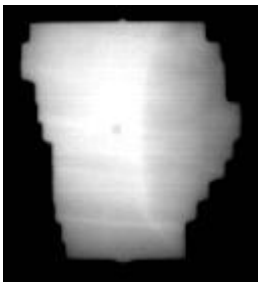 b) 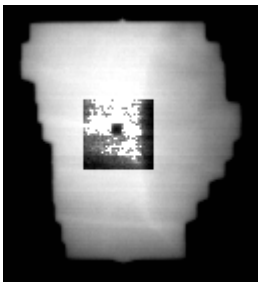

Figure 5 : Portal image of the phantom, obtained by a conventional EPID (Varian, Palo Alto, USA). The implanted marker is hardly perceptible in the image (a). Histogram equalization of the central part of the image highlights the marker (b).

Table 1. Estimation errors of target tracking in images of phantom. First three columns: exhaustive search with different similarity / disparity measures and constant block-size; SSD = Sum of Squared Differences, SAD = Sum of Absolute Differences (3), k = 2 and 1 respectively, CNV = Correlation Normalized by Variance (2). Next three columns: exhaustive search with CNV and different block-sizes. The last column: log-D step search with CNV.

error [mms]	SSD	SAD	CNV	10 × 10	16 × 16	40 × 40	log-D step
maximum	3.16	2.24	2.24	1.0	1.0	2.24	1.0
mean	0.91	0.84	0.65	0.52	0.56	0.64	0.56
cumulated	1.0	2.0	2.24	1.0	0.0	4.12	0.0

Precision of the tracking in the images of the phantom, with different combinations of search strategy and similarity (disparity) measure, is reported in (Tab.1). With an image resolution of 1 mm = 1 pixel, the mean value of absolute errors was comprised between 0.52 mm and 0.91 mm. These values are to be compared with the uncertainty of positioning of the table, equal to 1 mm. The correlation (2) performed slightly better than the disparity measures (3), hence it can be recommended for this application. Although it is approximately three times slower than the disparity measures, it still can be computed in real-time when combined with the log-D step strategy which gave as good as results as the exhaustive search. The cumulated error corresponds to the residual distance between the estimated and theoretical positions of the target after a complete breathing cycle. As expected, the best results were obtained for the blocks big enough to contain the entire target, but not too big. Indeed, the largest cumulated error (4.12 mm) occurred for a great block which could be regarded as

model of the background rather than of the target. All these errors were smaller than the uncertainty margins (5-15 mm) added by the expert to the tumoral volume perceptible in scanner images, when defining the irradiation zone in static cases. We reported here the details of the tests carried out on poorly contrasted images of the phantom, acquired with a conventional EPID. In the case of the image sequence of a patient with a marker stuck on the skin, the maximum error never exceeded 1 pixel, probably thanks to better quality of the images.

This means that portal images can be used for the purpose of pulmonary tumor tracking, provided that the tumor is perceptible in the images or that stable (non-migrating) markers can be implanted in clinical practice. The tumor tracking system presented in [SHI'99] was also based on the assumption that markers can be implanted in the pulmonary region, but used an additional imaging system with fluoroscopic cameras instead of an EPID.

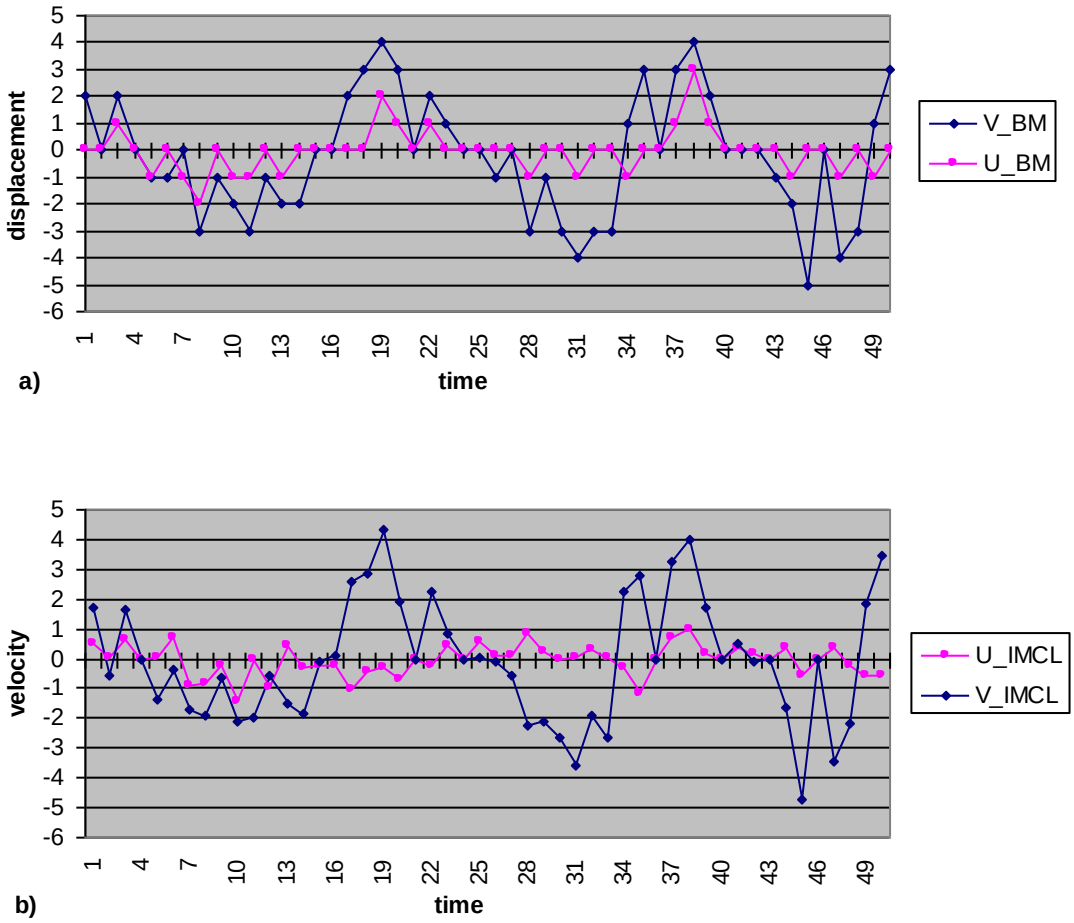

Figure 6 : Displacements (velocities) of the tumor from fig.2a, estimated by the BM algorithm (a) and by the IMCL algorithm (b). Displacements along the X-axis are negligible, while the displacements along the Y-axis show the same periodicity and magnitude in both graphs.

As mentioned above, according to a visual assessment the displacements in the image sequence without markers were correctly estimated by the BM algorithm (fig.6a). Hence they were used as reference for the assessment of the IMCL algorithm (fig.6b). As expected, the motion occurred mainly along the Y-axis. The displacements estimated by both algorithms are

very similar. Residual differences can be partly explained by the fact that the BM algorithm always provides integer values of the displacements along each axis, while the differential approach provides real values. It can be noticed that the overall trajectory, approximately corresponding to three breathing cycles, seems more accurate in the case of the IMCL algorithm (fig.7). Drift observed in the curve obtained by the BM algorithm may result from two phenomena. On the one hand, it can be a cumulated effect of truncation errors (integer values of the estimated displacements), because the reference block was updated from one image pair to another. On the other hand, the target tracking was performed on raw images, without compensation of the fluctuations of mean intensity. The method used to compensate these fluctuations is applicable to both algorithms and probably can still be improved.

Let us note that the displacements observed were relatively large, compared to the usual assumption of small displacements required by the differential approach. Indeed, this assumption is necessary for the validity of the motion constraint equation (4), which is based on a Taylor series expansion limited to the first order terms. Its validity range however is wider for low-contrast images with smooth variations of intensity. If necessary, larger displacements can be estimated within a multi-resolution scheme.

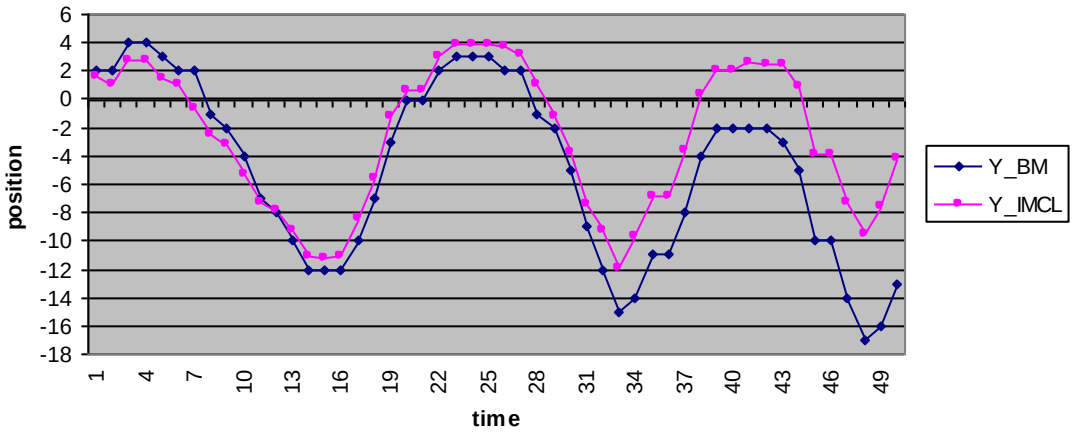

Figure 7 : Trajectories along the Y-axis obtained by integrating the velocities from fig.6.

Our experimentation shows that the BM algorithm is capable of tracking markers and tumors perceptible in portal images, while the IMCL algorithm is capable of estimating motion of perceptible tumors and of surrounding tissues in the absence of markers. Further experimentation with numerous image sequences is necessary to assess the power of both algorithms: limitations of their robustness, speed, ability of full automation (automatic choice of parameter values, initial detection of the target or of the region of interest *etc*.). The next step will be a clinical validation, but this requires a modification of a commercial radiotherapy equipment so as to control the relative position of the patient and of the treatment beam.

5. Conclusion

In our study, we applied conventional motion estimation and tracking algorithms in a new context of portal image sequences, to assess the possibility of tracking bronchial tumors during radiotherapy treatment. Unlike the existing methods designed to take into account these tumors' motion, our approach does not require any additional equipment compared to the standard radiotherapy setup. Despite very low contrasts in the portal images, our results

show that tracking of bronchial tumors' motion is feasible, using block-matching algorithms, provided that a radio-opaque marker is implanted in the tumor's vicinity. Such markers were already used by a competing Japanese team, but in a more complex setup with an additional fluoroscopic imaging system instead of the portal imaging device. Let us note however, that marker implanting is not yet available in the clinical context. Motion estimation without markers is more difficult. The conventional optical flow estimation approach using the smoothness constraint is not appropriate. However, our experimentation suggest that an algorithm based on intersections of motion constraint lines can provide satisfactory results. This algorithm takes into consideration a sparse set of points selected according to their spatio-temporal gradient values. The estimated displacements are supposed to be pure translations. This assumption is actually the same as in the case of block matching and it is compatible with the application. Indeed, the purpose of the motion estimation is to compensate the tumor's displacements. This can be done by moving either the table with the patient or the collimator leaves. Both can only undergo translational movements. Nevertheless, the motion estimation can also be used to re-evaluate *a posteriori* the actual radiation dose absorbed by the tissues. For this purpose, a more complex model of motion common to all the points, *e.g.* translation combined with zoom (affine model), may be necessary to take into account the expansion/contraction of the lungs. This still can be done using a sparse set of points selected according to same criteria of the spatio-temporal gradient values.

References

[AGG'81] J.K Aggarwal, L.S Davis, W.N Martin, Correspondence processes in dynamic scene analysis, *Proc. IEEE*, 69:5, 1981, pp 562-572

[ARM'98] J.G Armstrong, Target volume definition for three-dimensional conformal radiotherapy of lung cancer, *British Journal of Radiology*, 71, 1998, pp 587-594

[BAR'94] J.L Barron, D.J Fleet, S.S Beauchemin, Systems and experiment : performance of optical flow techniques, *Int. J. Computer Vision*, 12:1, 1994, pp 43-77

[CHU'89] C.H Chu, E.J Delp, Estimating displacement vectors from an image sequence, *J. Opt. Soc. Am. A*, 6:6, 1989, pp 871-878

[HOR'81] B.K.P Horn, B.G Schunck, Determining Optical Flow, *Artif. Intell*., 17, 1981, pp 185-203

[JAI'81] J.R Jain, A.K Jain, Displacement measurement and its application in interframe image coding. *IEEE Trans Comm*, COM.29, 1981, pp 1799-1808

[KUB'99] H.D Kubo, P.M Len, L Wang, B.R Leigh, H Mostafavi, Clinical experience of breathing synchronized radiotherapy procedure at the university of California Davis Cancer Center, Proceedings of the 41st Annual ASTRO Meeting , *Int. J. Radiation Oncology*, 45:3 supplement, 1999, p 204

[MAH'99] D Mah, J Hanley, K.E Rosenzweig, E Yorke, C.C Ling, S.A Leibel, Z Fuks, G.S Mageras, The deep inspiration breath-hold technique for the treatment of lung cancer: the first 200 treatments, Proceedings of the 41st Annual ASTRO Meeting , *Int. J. Radiation Oncology*, 45:3 supplement, 1999, p 204

[MOR'96] F Mornex, L'imagerie portale, pour quoi faire ?, *Bull. Cancer / Radiother*., 83, 1996, pp 391-396 (in French)

[MOR'99] F Mornex, P Giraud, P van Houtte, R Mirimanoff, O Chapet, P Loubeyre, Conformal radiotherapy of non-small-cell lung cancer, *Cancer Radiother*., 2:5, 1999, pp 425-436 (in French)

[ORK'96] M Orkisz, P Clarysse, Optical flow estimation preserving discontinuities : a survey, *Traitement du Signal*, 13:5, 1996, 489-513 (in French)

[ORK'99] M Orkisz, M Bourlion, G Gimenez, T.A Flam, Real-time target tracking applied to improve fragmentation of renal stones in extra-corporeal lithotripsy, *Machine Vision & Applications*, 11, 1999, 138-144

[ORK'98] M Orkisz, T Farchtchian, D Saighi, M Bourlion, N Thiounn, G Gimenez, B Debré, T.A Flam, Image-based renal stone tracking to improve efficacy in extra-corporeal lithotripsy, *J. Urol*., 160, 1998, 1237-1240

[SCH'89] B.G Schunck, Image flow segmentation and estimation by constraint line clustering, *IEEE Trans. PAMI*, 11:2, 1989, 1010-1027

[SHI'99] H Shirato, S Shimizu, T Shimizu, H Akita, N Kurauchi, N Shinohara, S Ogura, T Harabayashi, H Aoyama, K Miyasaka, Fluoroscopic real-time tumor tracking radiotherapy, Proceedings of the 41st Annual ASTRO Meeting, *Int. J. Radiation Oncology*, 45:3 supplement, 1999, p 205

[TIS'95] M. Tistarelli, Computation of coherent optical flow by using multiple constraints, Int. Conf. Computer Vision, Cambridge (MA), 1995, pp 263-268